Available online at BCREC website: https://bcrec.id

Bulletin of Chemical Reaction Engineering & Catalysis, 17 (3) 2022, 577-589

Research Article

# The Combined Effect of Bubble and Photo Catalysis Technology in BTEX Removal from Produced Water

**Marwah A. Al-Nuaim[1], Asawer A. Al-Wasiti[1]*, Zainb Y. Shnain[1], Abbas K. AL-Shalal[2]**

*[1]Chemical engineering, Department, University of Technology, Baghdad, Iraq.*
*[2]Training Center, Baghdad, Iraq*

*Received: 5th August 2022; Revised: 1st September 2022; Accepted: 2nd September 2022*
*Available online: 9th September 2022; Published regularly: September 2022*

## Abstract

Among the several ways used in wastewater treatment, the photocatalysis process is a more novel and alternative process that is increasingly employed in recent years. This work aims to improve the performance of the photocatalyst process by using air bubbles in removing the BTEX from produced water as an indicator of process efficiency. The study also shows the effect of influencing factors (pH and residence time) on the photocatalysis process. The study was done in a rectangular column with dimensions of 200 mm width, 30 mm depth, and 1500 mm height. Commercial titanium oxide ($TiO_2$) coated on a plate by the varnish was used as a source of the photocatalyst. The experiment was carried out under different values of gas flow rate (0-3 L/min) to evaluate its effect on the photocatalyst process, the effect of other variables of pH (3-11), and irradiation time (30-120) min was also studied. A new method of the coating was adopted by using an alumina plate with varnish as an adhesive. The characteristics results show that the coated plate has hydrophilic properties and that there is no significant change in the crystal structure of the $TiO_2$ nanoparticles and the varnish before and after 60 h of the photocatalytic process, indicating that the plate is still effective after 60 h usage under different conditions. The results also show that the introduction of air bubbles enhances the removal efficiency of BTEX significantly and the best removal effectiveness of BTEX was 93% when pH = 5 after 90 min and 90% when pH = 3 after 120 min. The removal rate also reached 86% when pH = 7 after 120 min all at a flow rate of 3 L/min. The percentage of removal decreased at pH = 9 and 11, reaching 64% and 50%, respectively after 120 min and a flow rate of 3 L/min .



***Keywords***: Photocatalytic process; air bubbles; coating; varnish; $TiO_2$; BTEX

***How to Cite***: M. Al-Nuaim, A.A. Al-Wasiti, Z.Y. Shnain, A.K. Al-Shalal (2022). The Combined Effect of Bubble and Photo Catalysis Technology in BTEX Removal from Produced Water. *Bulletin of Chemical Reaction Engineering & Catalysis*, 17(3), 577-589 (doi: 10.9767/bcrec.17.3.15367.577-589)

***Permalink/DOI***: https://doi.org/10.9767/bcrec.17.3.15367.577-589

## 1. Introduction

Produced water PW is defined as any water that exists in a reservoir that contains a hydrocarbon resource [1]. BTEX (benzene, toluene, ethylbenzene, and xylene) and low molecular weight hydrocarbons are the most abundant hydrocarbons in PW. The concentration of BTEX in untreated PW is around 600 mg/L under various storage conditions [2]. BTEX are volatile aromatic hydrocarbons. They are very toxic to both humans and the environment. The EPA (Environmental Protection Agency) classifies benzene ($C_6H_6$) as a hazardous aromatic hydrocarbon [3]. As a result, the oil and gas sector around the world has been pushed to advance water treatment technologies [4]. There are several therapy options for PW treatment. These

* Corresponding Author.
Email: asawer.a.alwasiti@uotechnology.edu.iq (A.A. Al-Wasiti)

approaches, which included physical, membrane, biological, chemical, and thermal treatments, enhanced oxidation processes and were offered as a result of their benefits [5]. The photocatalytic process is a novel and alternative method that is increasingly employed in water treatment due to its low cost, minimal intermediate product creation, and lack of secondary waste [6,7]. When the photocatalyst $TiO_2$ is attacked with photons from UV light, photocatalysis begins (from an artificial source or solar light). If the energy of these photons exceeds the band gap, the electrons ($e^-$) on the surface photocatalyst become "stimulated" in the valance band and move up into the conduction band (see Figure 1). A positive hole ($h^+$ VB) is created on the valence band once the $e^-$ has been absorbed into the conduction band ($e^-$ CB) (Equation (1)) [8]. In the conduction band ($e^-$ CB), the excited electrons combine with oxygen ($O_2$) to form superoxide radicals ($\cdot O_2^-$) or hydroperoxide radicals ($\cdot HO_2$), (Equation (2)) [9]. These reactive oxygen species are subsequently employed to break down contaminants into carbon dioxide ($CO_2$) and water ($H_2O$), as well as other secondary degradation processes. At the positive hole in the valance band ($h^+$ VB), where this reaction is happening, water is being oxidized. Equation (3) shows that this reaction produces hydrogen ions ($H^+$) and hydroxyl radicals ($\cdot OH$). The presence of contaminants causes the $\cdot OH$ to react, forming $H_2O$ and $CO_2$ [10].

$$TiO_2 + hv \rightarrow h^+_{VB} + e^-_{CB} \quad (1)$$

$$e^-_{CB} + O_2 \rightarrow \cdot O_2^- \quad (2)$$

$$h^+_{VB} + H_2O \rightarrow \cdot OH + H^+ \quad (3)$$

Several materials were used as a photocatalyst, these materials should be triggered by light, and exhibit a certain degree of thermal stability, low toxicity, and cheap cost. $TiO_2$ and ZnO are the most material that has such properties, they were extensively investigated and exploited in heterogeneous photocatalysis [11,12]. $TiO_2$ converts organic contaminants into $CO_2$, $H_2O$, and reactive oxidizing species such as oxygen or air during the photocatalytic process [13]. Figure (2a) depicts the number of papers on various semiconductors in the field of photocatalysis demonstrating the dominance of these two semiconductor oxides in this field of research. Additionally, various metals are connected with photocatalysis Figure (2b) to enhance photocatalyst performance. Aluminum and copper are the most often reported [14,15]. Some researchers have worked on removing the BTEX, the researchers [16] focused on UV-based advanced oxidation. In their work, they used batch reactor systems with UV/$H_2O_2$ to determine the removal efficiencies and the best conditions for photodegradation, The operating parameters for $H_2O_2$ (0.42, 0.72, 1.11, 1.34, and 1.736 g/L), pH ( 3-11), UV lights are 0.0001, 0.0002, and 0.0003 J/min.mL, The greatest rate of deterioration was seen after 30 minutes, and elimination was 98% at a pH of 3.1 under three UV lamps, BTEX (550-210 mg/L) [16].

In the work of Sheikholeslami *et al.* [17] Maghemite nanoparticles were utilized to eliminate the contaminants for the first time. By using a wet chemical process, maghemite was created as a semiconductor photocatalyst. Their study was done on the effects of the primary variables, such as pH (3-7), catalyst concentration (0-250 mg/L), and UV light intensity (0-100 W). Their results showed that the greatest BTEX removal effectiveness (82%) was achieved in 90 minutes at pH = 3, 170 mg/L of nanoparticles, and 100 W of UV radiation [17]. The same researcher uses the $\gamma$-$Fe_2O_3$ nanoparticle-based nano photocatalytic method, which

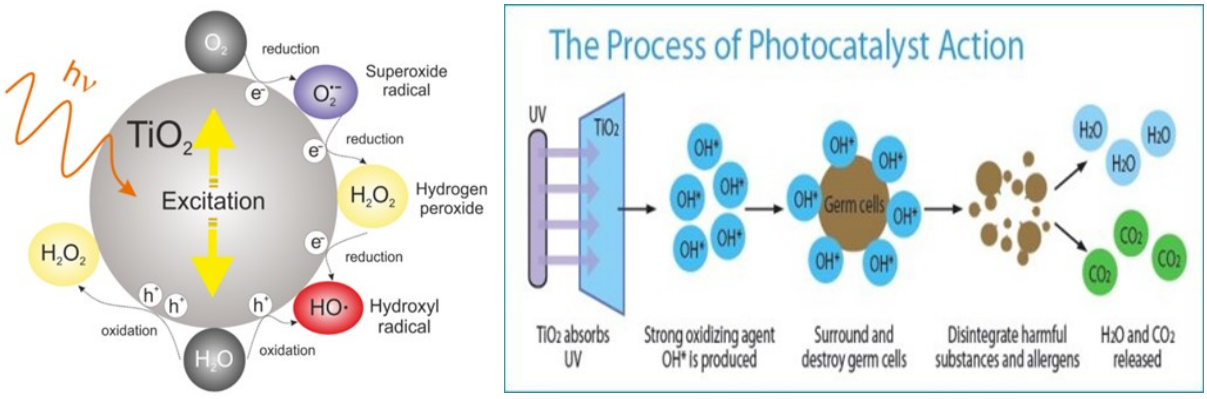


Figure 1. Photocatalytic mechanism [8]

has a high removal and degradation efficiency under different operating conditions. They found that the greatest BTEX removal effectiveness (90.94 %) was recorded at 3.64 pH, 167 mg/L of nanoparticle concentration, and 180 W of light intensity [18]. (S.A. Hasanova), determined how well BTEX from wastewaters degrades when exposed to ultraviolet (UV) and visible light (VIS). $TiO_2$ Nanopowder was the photocatalyst in this work. N-Doping, which required 97 % diethyl amine solution, was made from 20 % of that substance. The procedures were run at 293–323 K, with an irradiation duration range of 0–360 min, an initial pH range of 2–12, and a catalyst dosage of 0.1–2 mg/L. The 1 mg/L N-doped $TiO_2$ catalyst produced the best degradation of 91.6 % under the conditions of pH 3.5 after two hours [19]. Lotfi *et al.* [20] used a sol-gel approach to create the $UiO_{66}$-$NH_2$/$TiO_2$/ZnO (UTZ) nanocomposite as a photocatalyst to remove BTEX. Their results showed that the removal efficiency was 90.03 % under optimum conditions of pH = 7, concentration of 0.11 g/L, and 15 W light power.

Most of the above researchers used the catalyst directly as a powder and despite its effectiveness, the recovery of the catalyst requires the use of expensive membranes to separate the treated wastewater from the catalyst powder. Therefore, this work intended to solve this problem by using a fixed catalyst coated on the surface of the aluminum plate. Indeed, to improve the efficiency of the process and reduce its time, the air bubbles were examined at different flowrate. Accordingly, the aim of the work is to study the effectiveness of air bubbles in the removal of BTEX in UV-photo catalyst, where it was done under flow rates (0-3) L/min, as well as to study the effect of different variables of the pH (3-11) and irradiation time till two hours on the photocatalytic process by conducting COD examination.

## 2. Materials and Methods

### 2.1 Materials

All the materials used are in analytical grade as listed in Table 1.

### 2.2 Experimental Setup

The schematic experimental setup is shown in Figure 3. It consists of a rectangular column 200 mm width, 30 mm deep, 1500 mm high,

Table 1. Materials of research

| Chemical | Country | Purity (%) |
|---|---|---|
| Epoxy-type molto look | German | - |
| Varnish coating | UK | - |
| *Hydrochloric acid ( HCl)* | India | 35-38 |
| Sodium hydroxide (NaOH) | India | 98 |
| Benzene | UK | 99.5 |
| Toluene | India | 99.5 |
| Ethyl Benzene | Switzerland | 99 |
| Xylene | India | 99 |
| Titanium Oxide Nanoparticles/ Nanopowder ($TiO_2$ 99.5% purity with diameter 10-30nm) Anatase | USA | 99.5+ |
| Aluminum plate | Turkey | - |

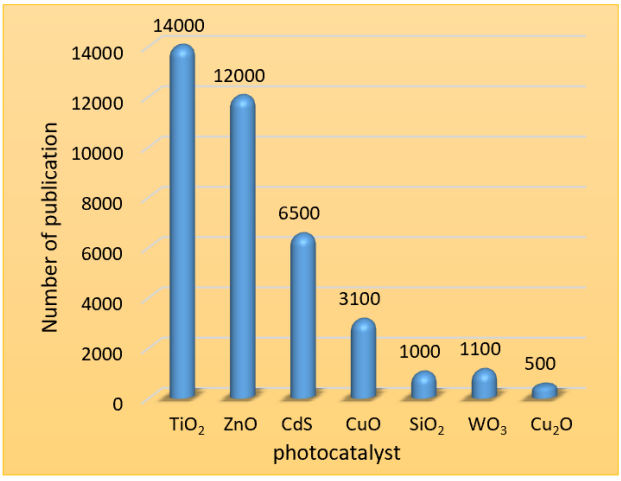


(a)

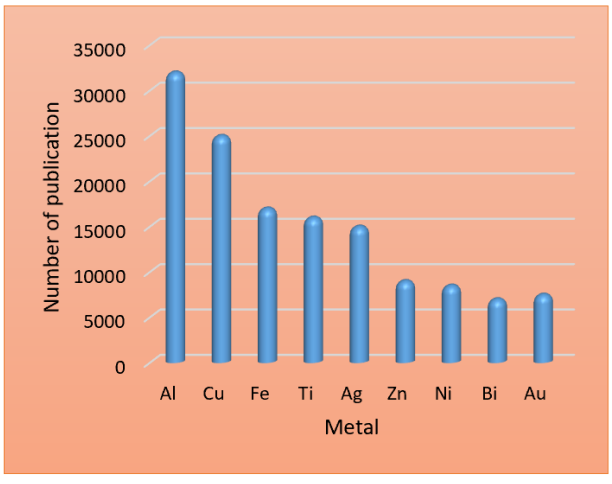


(b)

Figure 2. The number of publications about photocatalysts (a) and (b) metals used in photocatalysis. [14,15]

and 6 mm thick wall glass. At the bottom of the column, air enters through a gas distribution system comprising a total of 21 needles with a 5 mm square placed in the middle of the column bottom plate [21]. The inner diameter of the needles was 1 mm, the distributor was connected to the gas compressor (to supply the photo reactor with air) and the amount of air was controlled by the flow meter. The reactor was irradiated with a sterile tube with a UV lamp (tube-type germicidal UV light T5 (G5), W = 12 $m^2$, tube length 60 cm). The outer surface of the reactor and the UV lamp is covered with aluminum foil to prevent the interference of UV rays.

2.3 Plate Coating Method

An aluminum plate (dimensions 0.75 m long, 0.18 m width) was used as a base for catalyst coating. The plate was cleaned well using water and cleaning materials and left to dry, then it was sanded using sandpaper at 120 degrees to form grooves on it. Two methods were used to coat the plate, the first one was to coat the plate with epoxy by using a paintbrush evenly along with the plate and left to warm for one hour at room temperature, after the second layer of paint was added and left for half an hour. Titanium dioxide was prepared with an aqueous solution [5:1] of water and was mixed with a magnetic stirrer for 40 minutes. Then the plate was sprayed with a solution and left to dry for 48 h [22]. When using this method, an increase in the proportions of (COD) was observed. This is because epoxy contains organic materials, which led to an increase in the chemical need for oxygen.

Therefore, a second method was adopted by using varnish instead of epoxy, where the sheet was cleaned from dust and left to dry, then it was coated with a layer of varnish diluted with benzene and left for (15 minutes). Then a solution of $TiO_2$ was sprayed with distilled water and placed in the oven for (15 minutes) and left to cool for 4 h. After it was dried with hot air for 5 minutes, every four hours for two days.

2.4 Method and Test

The BTEX solution was prepared by adding (Benzene 0.33 g/L, Toluene 0.4 g/L, Ethyl Benzene 0.46 g/l, and Xylene 0.45 g/l) to two liters of water. The solution was mixed well by Ultrasound for 30 min. The pH values of the solution were adjusted at (3, 5, 7, 9, and11) by adding HCl for the acidic medium and (NaOH) for the basic medium. After preparing the solution it was added to the system (glass column) and the air was bubbled through the using flow meter at flow rate values of (1, 2, and 3) L/min. The ultraviolet ray was irradiated for a certain time of (30, 60, 90, and 120) min. Samples were taken for each irradiation time to calculate the

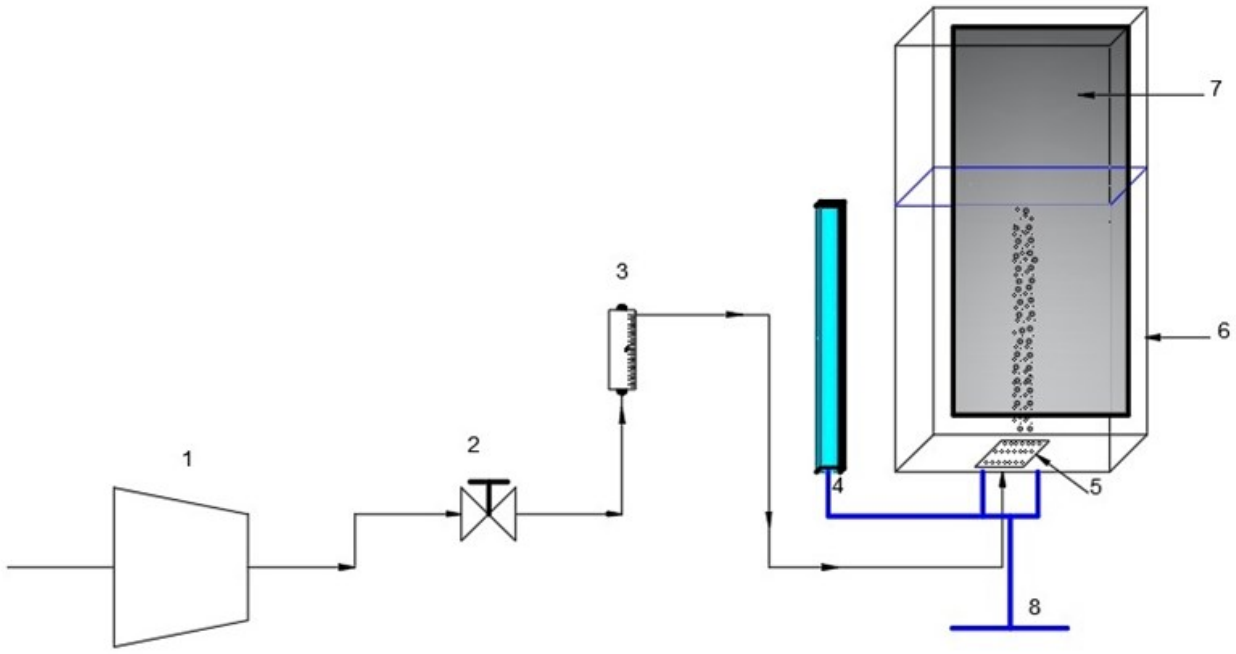


Figure 3. Experimental setup. (1) Air compressor. (2) Flow control valve. (3) flow meter. (4) lamp UV 250 nm. (5) Distributor (6) Column glass. (7) Aluminum plate fixed on it titanium dioxide ($TiO_2$). (8) stand

percentage removal of BTEX by measuring chemical oxygen demand (COD). The tests are carried out according to the restrictions of the Iraqi environment, where the allowable rate of COD is 100 ppm (Public Water and Rivers Conservation Law No. 25 of 1967) [23].

The coated plate was characterized by water contact angle (WCA), FTIR, and XRD tests. The water contact angle of $TiO_2$ particles and the coated plate was measured using the Standard Contact Angle Goniometer with DROP image [Model 200 Standard (p/n 200-U1), USA], the test was done by dripping a 5 µL drop of deionized water onto the catalyst particle (titanium dioxide/Anatase). The profile of the droplet placed on the substrate using a syringe and a mobile plate was recorded by a camera and analyzed by a computer to record the contact angle using Young's relationship

FTIR spectra were recorded in the scope of 4000 – 400 $cm^{-1}$ by utilizing FTIR spectrophotometer [Type, IRAffinity-1-SHMADZo Origin: Germany] with ATR technology. The XRD test was carried out with XRD analyzer (type: Philips PW1730/Netherlands) under the following specification; X-ray tube: Cu (1.54060 A), Voltage: 40.0 kV, Cu rent: 30.0 mA, Scan range: 10.000 <-> 90, 0000°, Step size: 0.2000°, Count Time: 1.20, DS Aperture Seconds: 1.00°, SS: 1.00°, RS: 0.30 mm.

## 3. Results and Discussion

### 3.1 Characterization of the Titanium Dioxide

#### 3.1.1 Contact angle measurement

A contact angle measurement test was done to examine the hydrophilicity of the surface of the produced $TiO_2$ with varnish. The water contact angle (WCA) was measured by dripping a 5 µL drop of deionized water onto the catalyst particle. A contact angle of 0° indicates total wetness which is the same angle that was recorded in Figure (4-a), which represents titanium dioxide/Anatase. Figure (4-b) illustrates the contact angle after the coating process using varnish and titanium at 69.9320° as a result of the hydrophilic surface of the plate with low surface energy and proper microstructure. The literature shows that a solid surface is hydrophilic if the water contact angle is less than 90 degrees. The solid surface is hydrophobic if the contact angle with water is more than 90 degrees. A contact angle of 0° indicates total wetness whereas a contact angle of 180° indicates total non-wetting [24]. When $TiO_2$ of the Anatase form is subjected to UV radiation, very low contact angles (less than 1o) are produced. These materials have the unusual ability to "attract" water rather than reject it (super-hydrophilicity). Instead of creating droplets, the water spreads out into flat sheets on the surface. The super-hydrophilic behavior of the $TiO_2$ surface is maintained for around two days if the illumination is interrupted. Furthermore, titanium dioxide exposed to UV light creates potent agents capable of oxidizing and decomposing a wide variety of microorganisms, organic compounds, and inorganic substances [25].

#### 3.1.2 Fourier Transform Infrared Spectroscopy (FTIR)

The FTIR is used to clarify the $TiO_2$ particle's functional groups as well as its chemical structures. The test was done on the coating

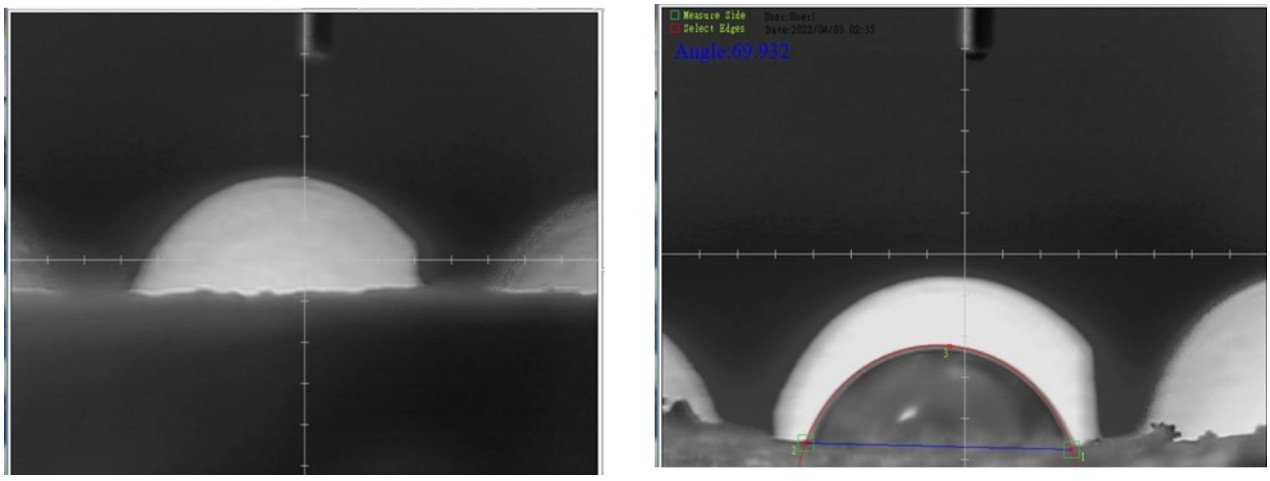


(a) (b)

Figure 4. Contact angle test, (a) the contact angle of $TiO_2$ nanoparticle/Anatase, (b) the contact angle of the coated plate with a layer of varnish and $TiO_2$

plate before and after the photocatalyst process as shown in Figures (5 (a) and (b)), respectively. The FTIR spectra were recorded in the scope of 4000–400 $cm^{-1}$. The spectra showed 3745.76 $cm^{-1}$, the peak observed around are due to the stretching vibration of the O–H group in figure (5a), while in Figure 5 (b) after using a plate for 60 h, the peaks identified at 3687.9 $cm^{-1}$ are due to the stretching and bending vibrations of (O–H), indicating no change between them. The peaks in the plate (3282.85, 3167.12, and 3062.96 $cm^{-1}$) are the strong broad corresponding to the hydroxyl group's symmetric and asymmetric stretching vibrations due to water molecules. is related to the O–H stretching mode of the hydroxyl group, indicating the presence of moisture in the sample [26].

The peaks observed on plate (a), 2920.23 and 2854.65 $cm^{-1}$, were due to the bending vibrations of the alkane (C–H) groups, the strong intensity of C–H peaks (2920.23 and 2850.80 $cm^{-1}$) becomes increased due to the increasing amount of modifying agent on its surface after 60 h of work (plate b). The merged peaks (2349.30 and 2214.28 $cm^{-1}$) are due to the stretching and bending vibrations in the (O=C=O), in the plate (a) became one peak stronger ( 2333.87 $cm^{-1}$) in the plate (b) [27]. Meanwhile, the peak of ester (C=O) was identified at 1735.94 $cm^{-1}$, and it did not change in plates (a and b).

The gradual group merging of amide in the plate (a) (1639.5, 1616.35, and 1597.06 $cm^{-1}$) to 1608.64 $cm^{-1}$, in the plate (b), indicates a

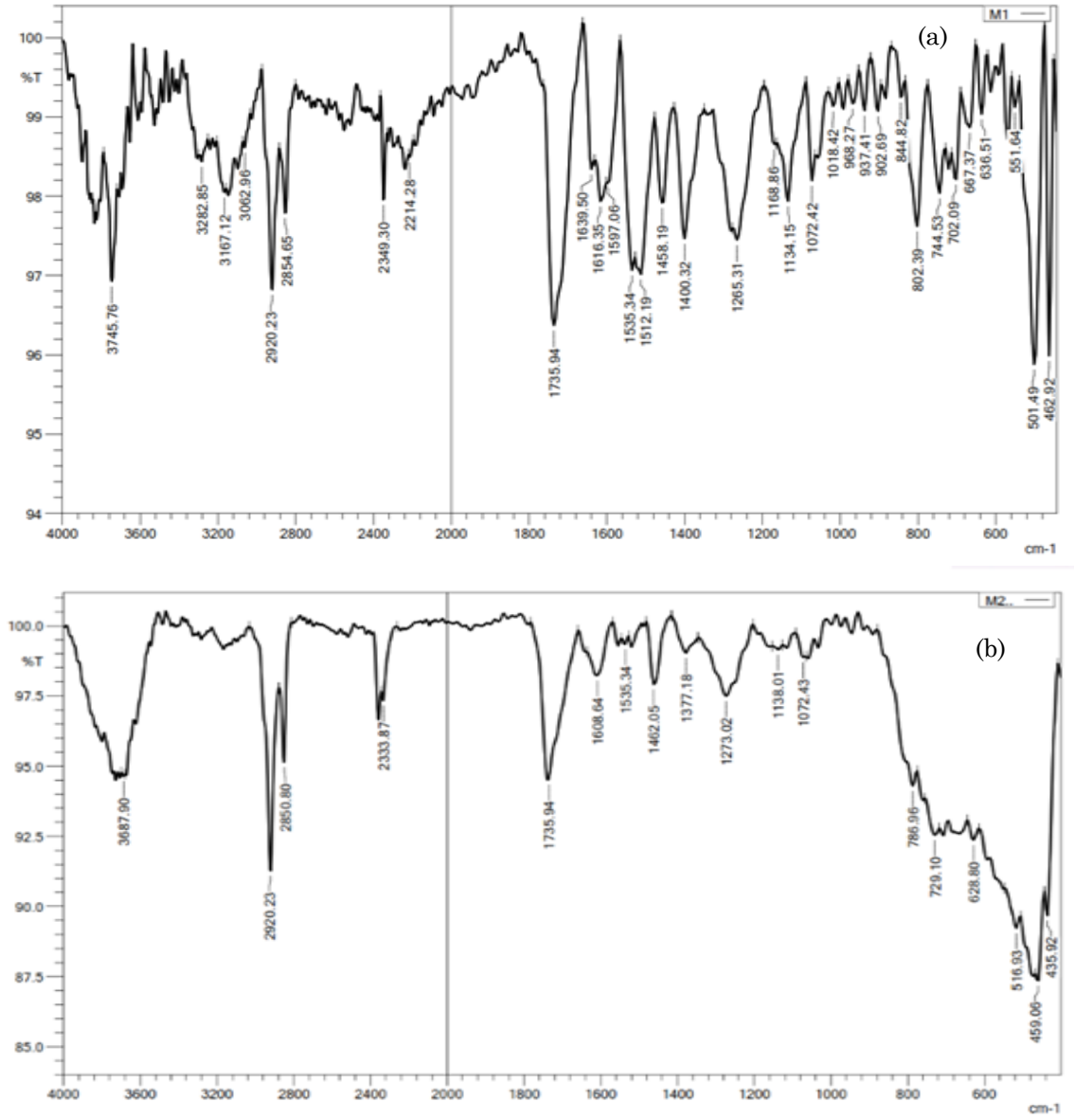


Figure 5. FTIR test for the coated plate, (a) Before using the plate, (b) after using the plate for 60 working hours

gradual removal and steep destruction of the amide group in the plate after 60 h [28]. The peaks at the (1535.34–1265.31 $cm^{-1}$) in the plate (a), and (1535.34–1273.02 $cm^{-1}$) in the plate (b) region could be attributed to the carboxyl (C=O) and methylene groups. The carboxyl and methylene groups might be also resulted from residual organic species [29].

Broadband from 1000 to 400 $cm^{-1}$ region is ascribed to the Ti–O stretching and Ti–O–Ti bridging stretching mode, For the pure $TiO_2$ in the range of 400–800 $cm^{-1}$, the peak at 462.92 $cm^{-1}$ in a plate (a) and 435.92 $cm^{-1}$ in a plate (b) should be attributed to the vibration of the Ti–O bond in the $TiO_2$ (Anatase titanium) lattice. The IR absorption band at 744.53 $cm^{-1}$ in a plate (a) and 729.10 $cm^{-1}$ in a plate (b) is attributed to the Ti–O–Ti stretching vibrations, This indicates that titanium dioxide is effective and present in the two plates, even after 60 hours of work [30], while varnish bands from (1018.42–802.39 $cm^{-1}$) in the plate (a) signalize the condensation reactions of varnish composite The reason of merging to (786.96 $cm^{-1}$) in plate (b) could be associated with a terpenic varnish, because it presents a considerable rate of aging, making these areas merge.

### 3.1.3 X-ray Diffraction (XRD) Characterization

The structure plate before and after the photocatalysis process was examined by X-ray diffraction, and the shape of the obtained XRD patterns revealed the state. The X-ray diffraction technique for the plate presented in Figures (6 a and b) was used to find out the amorphous and crystalline nature of the material of the coated plate before and after 60hr of the photocatalytic process, respectively. XRD patterns of $TiO_2$ nanoparticles and varnish are shown in Figure (6a) before using the plate showed firm diffraction peaks at 21, 25, 38.5, 42.5, 44.5, 65, and 78 which correspond to (400), (500), (600), (800), (24000), (8000), and (2200) respectively of nanoparticle $TiO_2$ Anatase and varnish.

After using the plate for 60 working hours under different operating conditions as shown in figure (6 b), it showed strong diffraction peaks at 22, 25.5, 38.5, 42, 45, 65, and 78 which correspond to (700), (1400), (3600), (400), (60000), (24000), and (5000) respectively of the Anatase $TiO_2$ nanoparticles and the varnish. The above results showed that after 60 working hours the crystal structure of $TiO_2$ fixed with varnish did not change.

The dispersion peak that appeared at 45 is attributed to the hydroxypropyl methylcellulose content in the natrosol component of varnish. regarding the $TiO_2$ nanoparticles in the varnish, the signals appeared weak at 25, 65, and 78. The weak signals of $TiO_2$ nanoparticles in the varnish are attributed to the loss of the quantity of the nanoparticles. Thus, the possibility of interaction between nanoparticles, resin, and new compounds is produced

It is noted from the two XRD tests before and after using the plate that there is no significant change in the crystal structure of the $TiO_2$ nanoparticles and the varnish, which indicates that the plate is still effective after 60 h of working under different conditions, and there is no reaction or change in the composition. of the coating material, which consists of $TiO_2$ nanoparticles and varnish.

### 3.2 Factors Influencing the Photocatalytic Reaction Process

#### 3.2.1 Effect of gas flow rate

To study the effect of airflow rate on the photocatalyst process, first, the behavior of the flow in the column should be understood.

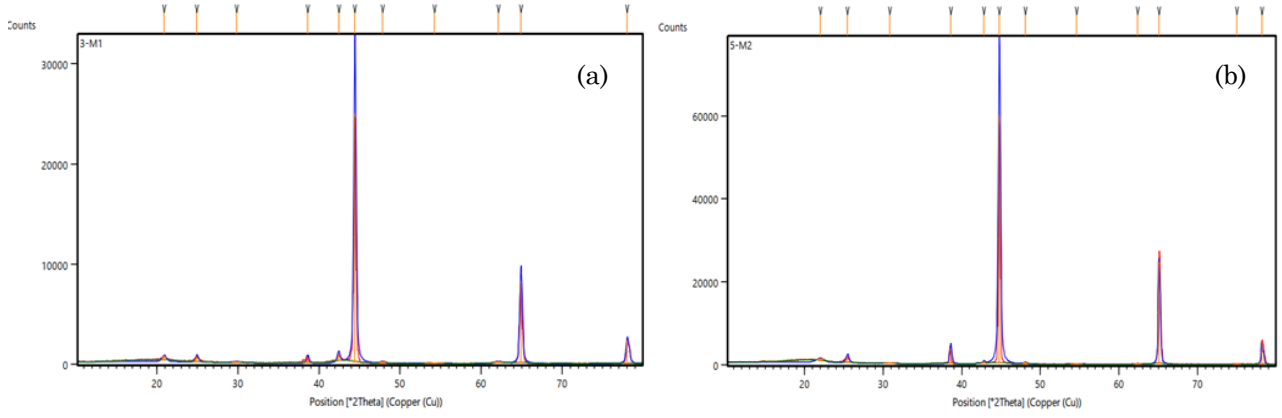


Figure 6. XRD test of the coated plate (a) before using the plate, (b) after using the plate for 60 working hours

Hence, Particle image velocimetry (PIV) is used to determine the flow and bubble behavior. A high-speed camera was fixed in front of the column and images were taken with a size of 20x20 cm. The number of bubbles and the rate of their diameter as calculated using Adobe Illustrator 2022. The results are shown in Table 2 and Figure 7.

The table shows that the higher the flow rate, the higher the number of bubbles and the smaller the average diameter. This is because with increasing the gas flow rate the fluid tends to be in turbulent flow leading to higher collision frequency and kinetic energy which affect the large bubbles by breaking up into two or more smaller bubbles. Bubble breakage generally depends on the balance between the external stresses that disrupt the bubble and the viscous stresses represented by the surface tension that resists bubble deformation. The majority of published breakup models are predicated on the same assumptions [31]: (a) Turbulent Eddies that strike the bubble surface and cause it to deform are what induce bubble breakup in a turbulent flow. The Eddies must possess enough energy to overcome the resisting forces to break up; (b) The Eddies ought to be smaller or equivalent to the bubble's size, while the eddies larger than the bubble transport the bubble only.

It was found from the visual observation that the bubbles are transported by the formed Eddies and vortices to their core. Meanwhile, due to the large dissipation energy of the turbulent flow of these vortices, the bubbles break up into small ones and this continues till that the break up reached zero because eddies that are smaller than the bubbles do not have enough energy to break them. It was also noticed that the smaller bubbles float up to the free surface due to buoyancy force.

Table 2. The number of bubbles and their average diameter

| Flow rate (L/min) | No . bubble | Average diameter (cm) |
|---|---|---|
| 1 | 43 | 0.78 |
| 2 | 54 | 0.63 |
| 3 | 101 | 0.59 |

The above effect of the ultra-high velocity of scattered air on the degradation of BTEX in the range (0-3 L/min) was tested and the results are presented in figures (8-12). A significant rise in the percentage of removal is observed with the increase in the ultra-high velocity of the air under the experimental conditions used in the present investigation. The best removal rate was at a flow rate of 3 L/min, where the removal rate of BTEX was 90% at pH 3, while the removal rate was 93% at pH 5, and 86% at pH 7 all at 120 minutes, while the flow rate did not make a difference at the mean baseline pH (9-11). It is also noted that when there is no air in the system the removal rate is very little and sometimes constant during the time of the experiments, which requires more time to obtain a high removal. This is can be attributed to the high velocity causing turbulent flow, as explained above and this led to enhancing the diffusivity of BTEX molecules to the active sites of the catalyst on the plate causing an enhancement in the rate of the degradation.

The other effect of the airflow rate is that those air bubbles function as a promoter by supplying molecular oxygen to the system. These oxygen molecules react with the free electrons, which are produced at the active sites on the catalyst surface under UV irradiation. As a result, additional hydroxyl radicals are produced according to the suggested degradation process (Equations (4)–(11) [32].

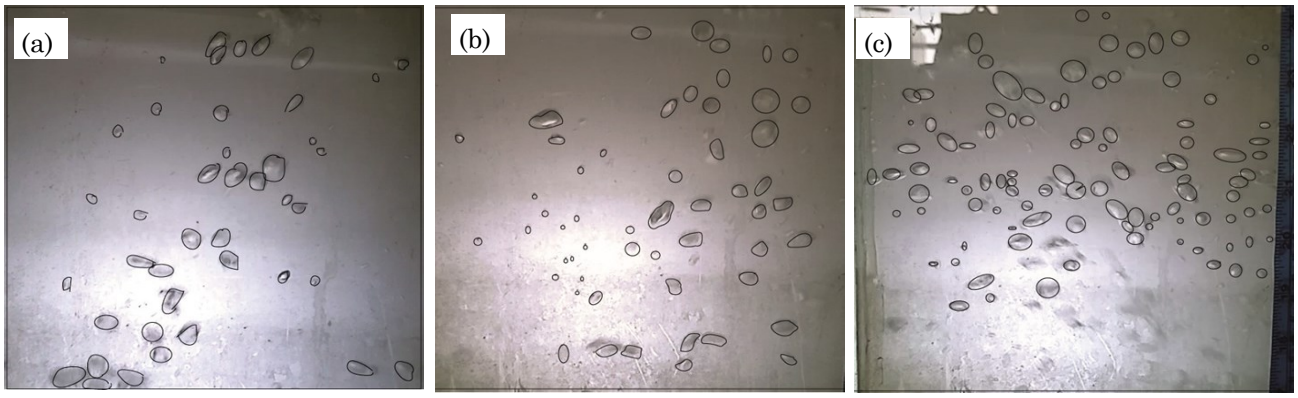


Figure 7. Images of bubbles at gas flow rates: (a) 1 L/min, (b) 2 L/min, and (c) 3 L/min

$$TiO_2 + \Delta Egab\ (UV) \rightarrow TiO_2\left(e^-_{CB} + h^+_{VB}\right) \quad (4)$$

$$TiO_2(h^+_{VB}) + H_2O \rightarrow TiO_2 + H^+ + OH^- \quad (5)$$

$$TiO_2(h^+_{VB}) + OH^- \rightarrow TiO_2 + OH^\bullet \quad (6)$$

$$TiO_2(e^+_{VB}) + O_2 \rightarrow TiO_2 + O_2^{\bullet-} \quad (7)$$

$$O_2^{\bullet-} + H^+ \rightarrow HO_2^{\bullet-} \quad (8)$$

$$2HO_2^\bullet \rightarrow H_2O_2 + O_2 \quad (9)$$

$$H_2O_2 + e^- \rightarrow OH^- + OH^\bullet \quad (10)$$

$$BTEX + OH^\bullet \rightarrow \text{degradation products} \quad (11)$$

Hence, the flow rate has a clear impact on the process of deterioration and removal of the pollutant, and the higher the flow rate, the less time necessary to scope the environmental limitation and reduce the time required.

3.2.2 Effect of pH

The removal efficiency of COD at different gas flows can be seen in Figures (13-16). These figures show that the best removal effectiveness was 93% when pH = 5 after 90 min, and 90% when pH= 3 after 120 min. The removal rate also reached 86% when pH = 7 after 120 min all of them are at a flow rate of 3 L/min. These results are consistent with those of earlier research [33]. Indeed, the percentage of removal decreased at 9 and 11, reaching 64% and 50%, respectively after 120 min and a flow rate of 3 L/min.

The disparate effect of pH on the BTEX removal can be attributed to the effect of pH on the charge of the catalyst particles, the aggregate size of the catalyst, and the locations of the conductance and valence bands. Due to the

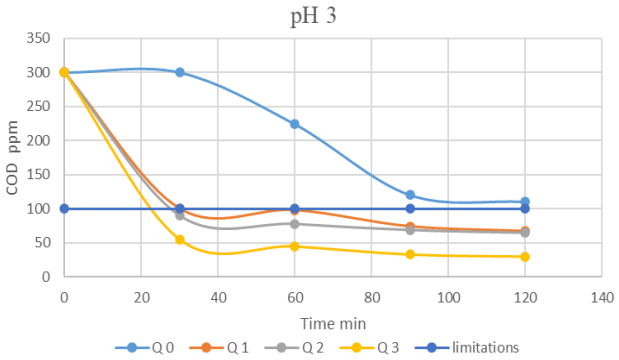


Figure 8. Relationship between time and COD at pH of 3

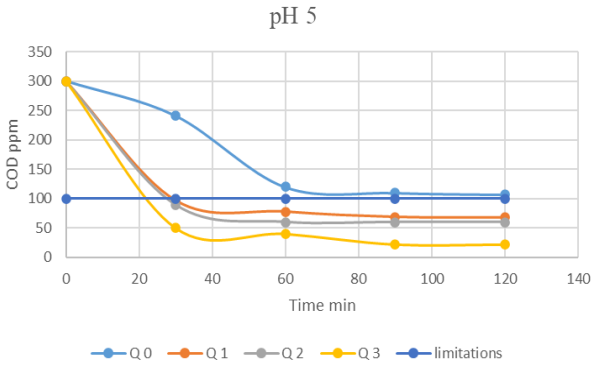


Figure 9. Relationship between time and COD at pH of 5

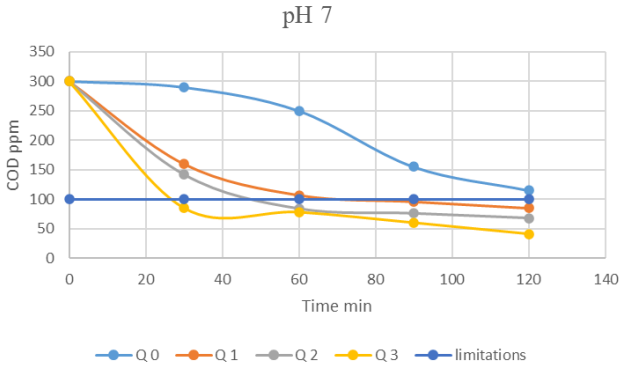


Figure 10. Relationship between time and COD at pH of 7

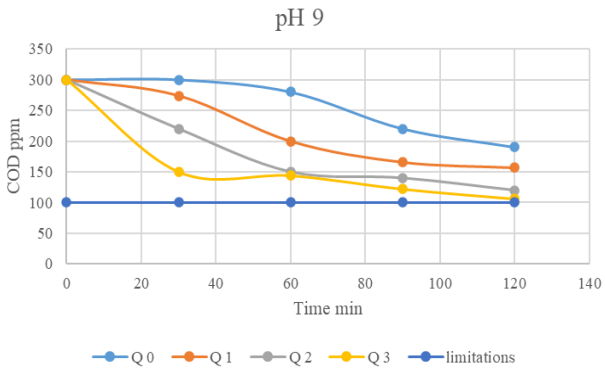


Figure 11. Relationship between time and COD at pH of 9

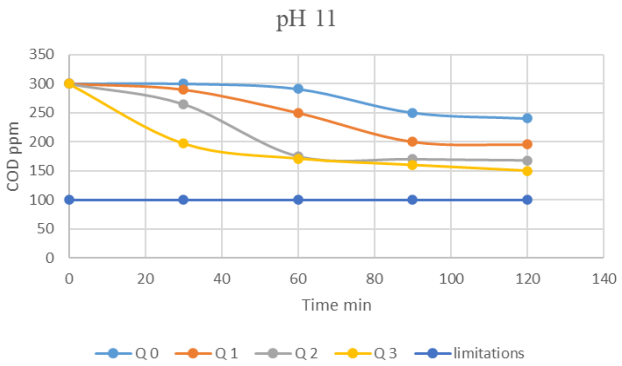


Figure12. Relationship between time and COD at pH of 11

nature of the $TiO_2$ catalyst utilized, any change in the operating pH is known to influence the photocatalyst's isoelectric point or surface charge. Numerous studies have employed $TiO_2$'s point of zero charges (PZC) to investigate the effect of pH on photocatalytic oxidation performance. The PZC condition is one in which the surface charge of $TiO_2$ is zero or neutral and its pH lies between 4.5 and 7.0, depending on the catalysts utilized. Because of the absence of an electrostatic force, the contact between the photocatalyst particles and water pollutants is low at the PZC of $TiO_2$. Since the pH PZC of $TiO_2$ is about 6.7 [34], titanium dioxide has a positive surface charge in an acidic media (pH less than 6.7) with the species of $TiOH_2^+$ and a negative charge in a basic media (pH greater than 6.7), with the species of $TiO^-$ as can be described by Equations (12) and (5) [35].

$$\text{At pH} < \text{PZC: } TiO + H^+ \leftrightarrow TiOH_2^+ \quad (12)$$

$$\text{At pH} > \text{PZC: } TiOH + OH^- \leftrightarrow TiO^- + H_2O \quad (13)$$

Operating with pH < PZC ($TiO_2$) (pH = 3, 5, and 7) the catalyst's surface charge becomes positively charged, exerting an electrostatic attraction force between $TiO_2$ and the anionic charged of organic molecules and this enhances the adsorption onto the photon-activated $TiO_2$ surface, facilitating subsequent photocatalytic processes [36]. Whilst in the basic solutions (pH > PZC ($TiO_2$) (pH = 9 and 11)), the catalyst's surface charge becomes negative, causing repulsion between the $TiO_2$ and anionic molecules and this will reduce the degradation process.

Hence, the change in pH has a substantial influence on the efficacy of BTEX clearance. By lowering the pH of the solution, the removal efficiency rises. Each change in operating pH influences the catalyst's isoelectric point or superficial load, the positive charge of the catalyst attracts more anions, causing an increase in the removal rate [36]. The oscillations in the curves (Figures 13-16) indicate that the primary cause for this process is the transformation of BTEX into intermediate products. which results in a rise in COD during the test and removal efficiency. Due to the varying test circumstances, several intermediate compounds are created and eliminated at varying periods, each with its unique COD. The efficiency of COD removal will be altered throughout the early hours of the test.

Finally, in the acidic range, the removal efficiency was at its highest value, so the effective pH range was in the range of 3 to 7, and the residence time worked from 30 to 120 minutes while the best removal rate was at a flow rate of 3 L/min. As for the basic medium, there is no removal, meaning that the photocatalytic process does not work in the pH range (9-11).

### 3.2.3 Irradiation time

The effect of irradiation time on the photolysis of BTEX is represented in Figures (9-12). It is noted that with the increase in the irradiation time up to 120 minutes, the rate of decomposition increases. For pH of 3 and 5 and using air bubbles, the rate of decomposition, after 30 min, was enough to reduce the BTEX concentration under the Iraqi limitation. Increasing the time by more than 30 min causes an increase in the removal rate from 83% to 93% at pH of 5 and 81% to 90% at pH of 3 and 71% to 86% at pH of 7 and flow rate of 3 L/min. This is because with an increase in the irradiation period the number of photons absorbed rises, cre-

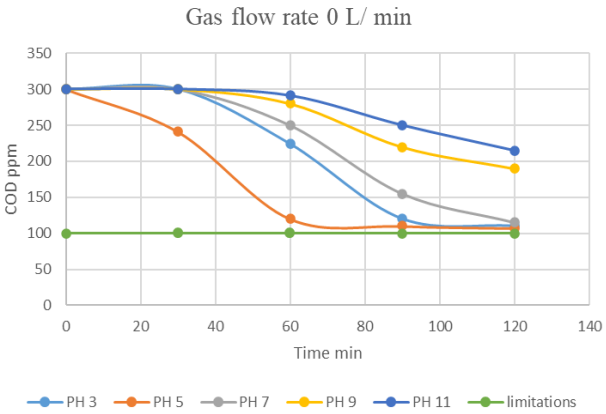


Figure 13. Relationship between time and COD at flow rate of 0 L/min

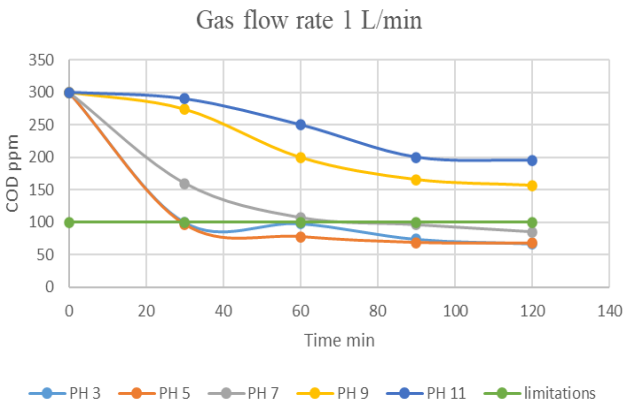


Figure 14. Relationship between time and COD at flow rate of 1 L/min

ating a larger quantity of OH· by promoting the oxidation of BTEX.

Whilst the decomposition rate remains constant at a time (30 - 90 - 120) in the operational conditions of pH of 3 and flow rate of 2 L/min in which the removal percentage reached 78%, while it stabilized at 80% at pH of 5 and flow rate of 1 L/min The reason for stability is due to the saturation of the surface This phenomenon might be explained by the fact that the dissolved $O_2$ molecules are supplied from the gas phase quicker than they are destroyed by diffusion from the aqueous layer covering the catalyst surface.

Indeed, the reaction rate reduces with irradiation duration as a result of the pseudo-first-order kinetics, and competition for degradation between the reactant and intermediate products. The challenges associated with reacting short-chain aliphatic with •OH radicals, as well as the photocatalyst's limited lifespan owing to active site deactivation by strong by-products deposition, contribute to the degradation's sluggish kinetics after a certain time limit [38].

## 4. Conclusion

In this work, the effective range of important parameters in the photocatalytic process of BTEX degradation by $TiO_2$ under ultraviolet was studied via the COD test. A new coating method of $TiO_2$ on the aluminum plate using varnish was adopted, the method is a simple and cheap in price for being easy to prepare. The characteristics tests show that the plate was not damaged after 60 working hours. The results show that the higher the flow velocity, the greater the removal rate, as the largest removal rates occurred at 3 L /min. The enhancement in removing BTEX with increasing gas flow rate is attributed to two reasons, the first enhancing the mobility and diffusion of BTEX molecules towards the active sites of the catalyst. The second effect is to enhance active OH generation. The greatest removal efficiency was 93% when pH = 5 after 90 minutes, and 90% when pH = 3 after 120 minutes. The removal efficiency was highest in the acid range in which the effective pH range was 3 to 7, and the treatment process lasted 30 to 120 minutes at a flow rate of 3 L/min. While, there is no removal in the basic media at pH (9 and 11). Finally, increasing the time increases the decomposition rate till it remains constant with the progression of time as a result of surface saturation and a significant reduction in the concentration. The Iraqi environmental limitation (than 100 ppm) was reached in most of the experiments after only 30 minutes from the start of the experiment, and with the progression of time, the percentage of removal increased.

## Acknowledgement

The authors would like to thank the Chemical Engineering Department, University of Technology, Iraq for supporting to complete this work.

## References

[1] Veil, J.A., Puder, M.G., Elcock, D., Redweik, RJ Jr. ( 2004). A white paper describing produced water from production of crude oil, natural gas, and coal bed methane. Lemont: Argonne National Lab.

[2] Lee, K., Neff, J. (2011). Produced water: environmental risks and advances in mitigation technologies. Berlin: Springer.

[3] Akmirza, I., Pascual, C., Carvajal, A., Pe´rez, R., Mun˜oz, R., Lebrero, R. (2017). Anoxic biodegradation of BTEX in a biotrickling filter. *Sci. Total Environ.* 587 (4), 57–65, DOI: 10.1016/j.scitotenv.2017.02.130

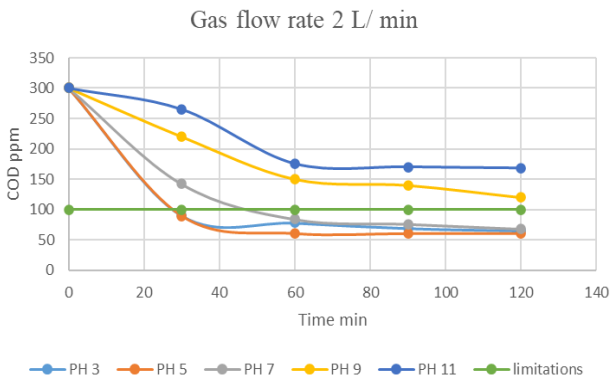


Figure 15. Relationship between time and COD at flow rate of 2 L/min

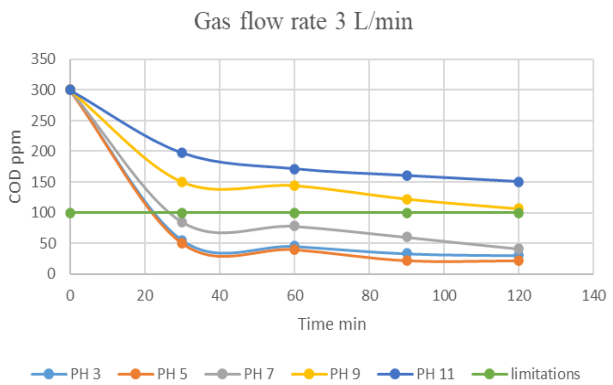


Figure 16. Relationship between time and COD at flow rate of 3 L/min

[4] Lu, J., Wang, X., Shan, B, Li, X, Wang, W. (2006) Analysis of chemical compositions contributable to chemical oxygen demand (COD) of oilfield produced water. *Chemosphere*, 62 (3), 22–31, DOI: 10.1016/j.chemosphere.2005.04.033

[5] Jime´nez, S., Mico´, M.M., Arnaldos, M., Medina, F., Contreras, S. (2018) State of the art of produced water treatment. *Chemosphere,* 192, 186–208, DOI: 10.1016/j.chemosphere.2017.10.139

[6] Dewil, R., Mantzavinos, D., Poulios, I., Rodrigo, M.A. (2017). New perspectives for advanced oxidation processes. *J. Environ. Manag*. 195, 93–99, DOI: 10.1016/j.jenvman.2017.04.010

[7] Chong, M.N., Jin, B., Chow, C.W., Saint, C. (2010). Recent developments in photocatalytic water treatment technology: a review. *Water Res*. 44, 2997–3027, DOI: 10.1016/j.watres.2010.02.039

[8] Shahrezaei, F., Mansouri, Y., Zinatizadeh, A.A.L., Akhbari, A. (2012) Process modeling and kinetic evaluation of petroleum refinery wastewater treatment in a photocatalytic reactor using $TiO_2$ nanoparticles. *Powder Technol*. 221, 203–212, DOI: 10.1016/j.powtec.2012.01.003

[9] Liu, B., Chen, B., Zhang, B. (2017). Oily wastewater treatment by nanoTiO2-induced photocatalysis: seeking more efficient and feasible solutions. *IEEE Nanatechnol. Mag*. 11,4–15, DOI: 10.1109/MNANO.2017.2708818

[10] Byrne, C., Subramanian, G., Pillai, S.C. (2017). Recent advances in photocatalysis for environmental applications. *J. Environ. Chem. Eng*., 6(3), 3531-3555, DOI: 10.1016/j.jece.2017.07.080.

[11] Lu, M. (2013). Photocatalysis and water purification: from fundamentals to recent applications. Hoboken: Wiley.

[12] Cervantes, T.N.M., Zaia, D.A.M., de Santana, H. (2009). Estudo da fotocatálise heterogênea sobre Ti/$TiO_2$ na descoloração de corantes sintéticos. *Quim. Nova*., 32, 2423–2428. DOI: 10.1590/S01004042200900900035

[13] Zolfaghari, M. (2019) .Propose for Raman mode position for Mn-doped ZnO nanoparticles. *Phys. B Phys. Condens. Matter.* 555, 1–8, DOI: 10.1016/j.physb.2018.11.072

[14] Lee, K.M., Lai. C.W., Ngai. K.S., Juan, J.C. (2016). Recent developments of zinc oxide based photocatalyst in water treatment technology: a review. *Water Res*., 88,428–448, DOI: 10.1016/j.watres.2015.09.045

[15] Frederichi, D., Scaliante, M.H.N.O., Bergamasco, R. (2021). Structured photocatalytic systems: photocatalytic coatings on low-cost structures for treatment of water contaminated with micropollutants - a short review. *Environmental Science and Pollution Research*, 28(19), 23610-23633. DOI: 10.1007/s11356-020-10022-9

[16] Bahmani, M., Bitarafhaghighi, V., Badr, K., Keshavarz, P., Mowla, D. (2014). The photocatalytic degradation and kinetic analysis of BTEX components in polluted wastewater by UV/$H_2O_2$- based advanced oxidation, *Desalination and Water Treatment*, 20, 52, 3054–3062, DOI: 10.1080/19443994.2013.797369

[17] Sheikholeslami, Z., Yousefi Kebria, D., Qaderi, F. (2018). Nanoparticle for degradation of BTEX in produced water; an experimental procedure, *Journal of Molecular Liquids,* 264, 476–482, DOI: 10.1016/j.molliq.2018.05.096

[18] Sheikholeslami, Z., Yousefi Kebria, D., Qaderi, F. (2020). Application of γ-$Fe_2O_3$ nanoparticles for pollution removal from water with visible light, *Journal of Molecular Liquids*, 299, 112-118, DOI: 10.1016/j.molliq.2019.112118

[19] Hasanova, S.A. (2021). Compared the Efficiency of $TiO_2$ and N-doped $TiO_2$ to Degrade BTEX, *Advanced Physical Research*, 3 (3), 123-128.

[20] Lotfi, H., Heydarinasab, A., Mansouri, M., Hossein Hosseini, S. (2022). Kinetic modeling of removal of aromatic hydrocarbons from petroleum wastewaters by UiO-66-$NH_2$/$TiO_2$/ZnO nanocomposite, *Journal of Environmental Chemical Engineering*. 10(1), 107066, DOI: 10.1016/j.jece.2021.107066

[21] Darmana, D., Henket, R.L.B., Deen, N.G. (2007). Detailed modelling of hydrodynamics, mass transfer and chemical reactions in a bubble column using a discrete bubble model: Chemisorption of $CO_2$ into NaOH solution, numerical and experimental study. *Chemical Engineering Science,* 62, 2556–2575, DOI: 10.1016/j.ces.2007.01.065

[22] Sriwong, C., Wongnawa, S., Patarapaiboolchai, O. (2012). Rubber sheet strewn with $TiO_2$ particles: photocatalytic activity and recyclability. *Journal of Environmental Sciences*, 24(3), 464-472, DOI: 10.1016/S1001-0742(11)60794-8.

[23] Anonym, (1967). Regulation of the maintenance of rivers and public waters from pollution No. (25) for the year 1967.

[24] Jansson, I., Garcia-Garcia, F.J., Sanchez, B. (2021). Key factors to develop hybrid photoactive materials based on mesoporous carbon/$TiO_2$ for removal of volatile organic compounds in air streams, *Applied Catalysis A: General*, 623, 118281, DOI: 10.1016/j.apcata.2021.118281

[25] Dikkar, H., Kapre, V., Diwan, A., Sekar, S.K. (2021). Titanium dioxide as a photocatalyst to create self-cleaning concrete, *Materials Today: Proceedings,* 45, 4058–4062, DOI: 10.1016/j.matpr.2020.10.948

[26] Shnain, Z.Y., Abid, M.F., Sukkar, K.A. (2021) Photodegradation of mefenamic acid from wastewater in a continuous flow solar falling film reactor, *Desalination and Water Treatment*, 210, 22–30, DOI: 10.5004/dwt.2021.26581

[27] Tarmizi, Z.I., Maski, A.N., Ali, R.R., Jusoh, N. W.C., Akim, A.M., Eshak, Z., Md Noor, S., Ibrahim, N. (2019). Fabrication of hydrophilic silica coating varnish on pineapple peel fiber based biocomposite. *International Journal of Integrated Engineering*, 11(7), 77-82,

[28] Farmakalidis, H.V., Boyatzis, S., Douvas, A.M., Karatasios, I., Sotiropoulou, S., Argitis, P., Chryssoulakis, Y., Kilikoglou, V. (2017). The effect of $TiO_2$ component on the properties of acrylic and urea-aldehyde resins under accelerated ageing conditions. *Pure and Applied Chemistry*, 89(11), 1659-1671, DOI: 10.1515/pac-2016-1220

[29] Praveen, P., Viruthagiri, G., Mugundan, S. (2014). Structural optical and morphological analyses of pristine titanium di-oxide nanoparticles – Synthesized via sol–gel route, *Spectrochimica Acta Part A: Molecular and Biomolecular Spectroscopy,* 117, 622–629, DOI: 10.1016/j.saa.2013.09.037

[30] Porkodi, K., Arokiamary, S.D. (2007). Materials Characterization Synthesis and spectroscopic characterization of nanostructured anatase titania: A photocatalyst, *Materials Characterization,* 58 (2007), 495–503, DOI: 10.1016/j.matchar.2006.04.019

[31] Abdellah, M.H., Nosier, S.A., El-Shazly, A.H., Mubarak, A.A. (2018) Photocatalytic decolorization of methylene blue using $TiO_2$/UV system enhanced by air sparging, *Alexandria Engineering Journal*, 57 (4), 3727-3735, DOI: 10.1016/j.aej.2018.07.018

[32] Shahrezaei, F., Mansouri, Y., Zinatizadeh, A.A.L., Akhbari, A. (2012) Process modeling and kinetic evaluation of petroleum refinery wastewater treatment in a photocatalytic reactor using $TiO_2$ nanoparticles. *Powder Technol.*, 221, 203–212, DOI: 10.1016/j.powtec.2012.01.003

[33] Jouali, A., Salhi, A., Aguedach, A., Aarfane, H., Ghazzaf, E., Lhadi, K., Tahiri, S. (2019) Photo-catalytic degradation of methylene blue and reactive blue 21 dyes in dynamic mode using $TiO_2$ particles immobilized on cellulosic fibers. *Journal of Photochemistry and Photobiology A: Chemistry,* 383, 112013, DOI: 10.1016/j.jphotochem.2019.112013

[34] Kavil, Y.N., Shaban, Y.A., Alelyani, S.S., Al-Farawati, R., Orif, M.I., Ghandourah, M.A., Schmidt, M., Turki, A.J., Zobidi, M. (2020). The removal of methylene blue as a remedy of dye-based marine pollution: a photocatalytic perspective. *Research on Chemical Intermediates,* 46 (1), 755-768, DOI: 10.1007/s11164-019-03988-w

[35] Chong, M.N., Lei, S., Jin, B., Saint, C., Chow, C.W.K. (2009). Optimisation of an annular photoreactor process for degradation of Congo red using a newly synthesized titania impregnated kaolinite nano-photocatalyst. *Sep. Purif. Technol.*, 67, 355-363, DOI: 10.1016/j.seppur.2009.04.001

[36] Alwasiti, A.A., Shnain, Z.Y., Abid, M.F., AbdulRazak, A.A., Abdulhussein, B.A., Mahdim, G.S. (2021) Experimental and numerical study on the degradation of mefenamic acid in a synthetic wastewater, *IOP Conf. Series: Earth and Environmental Science*, 779, 012073, DOI: 10.1088/1755-1315/779/1/012073

[37] Khasawneh, O.F., Palaniandy, P. (2020). Removal of organic pollutants from water by $Fe_2O_3$/$TiO_2$ based photocatalytic degradation: A review. *Environmental Technology and Innovation*, 101230, DOI: 10.1016/j.eti.2020.101230

[38] El-Tawargy, A.S. (2022) Spatio-temporal photolysis rate profiles of UV254 irradiated toluene. *Scientific Reports*, 12(1), 1-10. DOI: 10.1038/s41598-022-16941-6.